

Proceedings of the 12th International Conference on
Computational Fluid Dynamics in the Oil & Gas,
Metallurgical and Process Industries

Progress in Applied CFD – CFD2017



SINTEF Proceedings

Editors:

Jan Erik Olsen and Stein Tore Johansen

Progress in Applied CFD – CFD2017

Proceedings of the 12th International Conference on Computational Fluid Dynamics
in the Oil & Gas, Metallurgical and Process Industries

SINTEF Academic Press

SINTEF Proceedings no 2

Editors: Jan Erik Olsen and Stein Tore Johansen

Progress in Applied CFD – CFD2017

Selected papers from 10th International Conference on Computational Fluid Dynamics in the Oil & Gas, Metallurgical and Process Industries

Key words:

CFD, Flow, Modelling

Cover, illustration: Arun Kamath

ISSN 2387-4295 (online)

ISBN 978-82-536-1544-8 (pdf)

© Copyright SINTEF Academic Press 2017

The material in this publication is covered by the provisions of the Norwegian Copyright Act. Without any special agreement with SINTEF Academic Press, any copying and making available of the material is only allowed to the extent that this is permitted by law or allowed through an agreement with Kopinor, the Reproduction Rights Organisation for Norway. Any use contrary to legislation or an agreement may lead to a liability for damages and confiscation, and may be punished by fines or imprisonment

SINTEF Academic Press

Address: Forskningsveien 3 B
 PO Box 124 Blindern
 N-0314 OSLO

Tel: +47 73 59 30 00

Fax: +47 22 96 55 08

www.sintef.no/byggforsk

www.sintefbok.no

SINTEF Proceedings

SINTEF Proceedings is a serial publication for peer-reviewed conference proceedings on a variety of scientific topics.

The processes of peer-reviewing of papers published in SINTEF Proceedings are administered by the conference organizers and proceedings editors. Detailed procedures will vary according to custom and practice in each scientific community.

PREFACE

This book contains all manuscripts approved by the reviewers and the organizing committee of the 12th International Conference on Computational Fluid Dynamics in the Oil & Gas, Metallurgical and Process Industries. The conference was hosted by SINTEF in Trondheim in May/June 2017 and is also known as CFD2017 for short. The conference series was initiated by CSIRO and Phil Schwarz in 1997. So far the conference has been alternating between CSIRO in Melbourne and SINTEF in Trondheim. The conferences focuses on the application of CFD in the oil and gas industries, metal production, mineral processing, power generation, chemicals and other process industries. In addition pragmatic modelling concepts and bio-mechanical applications have become an important part of the conference. The papers in this book demonstrate the current progress in applied CFD.

The conference papers undergo a review process involving two experts. Only papers accepted by the reviewers are included in the proceedings. 108 contributions were presented at the conference together with six keynote presentations. A majority of these contributions are presented by their manuscript in this collection (a few were granted to present without an accompanying manuscript).

The organizing committee would like to thank everyone who has helped with review of manuscripts, all those who helped to promote the conference and all authors who have submitted scientific contributions. We are also grateful for the support from the conference sponsors: ANSYS, SFI Metal Production and NanoSim.

Stein Tore Johansen & Jan Erik Olsen



Organizing committee:

Conference chairman: Prof. Stein Tore Johansen

Conference coordinator: Dr. Jan Erik Olsen

Dr. Bernhard Müller

Dr. Sigrid Karstad Dahl

Dr. Shahriar Amini

Dr. Ernst Meese

Dr. Josip Zoric

Dr. Jannike Solsvik

Dr. Peter Witt

Scientific committee:

Stein Tore Johansen, SINTEF/NTNU

Bernhard Müller, NTNU

Phil Schwarz, CSIRO

Akio Tomiyama, Kobe University

Hans Kuipers, Eindhoven University of Technology

Jinghai Li, Chinese Academy of Science

Markus Braun, Ansys

Simon Lo, CD-adapco

Patrick Segers, Universiteit Gent

Jiyuan Tu, RMIT

Jos Derksen, University of Aberdeen

Dmitry Eskin, Schlumberger-Doll Research

Pär Jönsson, KTH

Stefan Pirker, Johannes Kepler University

Josip Zoric, SINTEF

CONTENTS

PRAGMATIC MODELLING	9
On pragmatism in industrial modeling. Part III: Application to operational drilling	11
CFD modeling of dynamic emulsion stability	23
Modelling of interaction between turbines and terrain wakes using pragmatic approach	29
FLUIDIZED BED	37
Simulation of chemical looping combustion process in a double looping fluidized bed reactor with cu-based oxygen carriers.....	39
Extremely fast simulations of heat transfer in fluidized beds.....	47
Mass transfer phenomena in fluidized beds with horizontally immersed membranes	53
A Two-Fluid model study of hydrogen production via water gas shift in fluidized bed membrane reactors	63
Effect of lift force on dense gas-fluidized beds of non-spherical particles	71
Experimental and numerical investigation of a bubbling dense gas-solid fluidized bed	81
Direct numerical simulation of the effective drag in gas-liquid-solid systems	89
A Lagrangian-Eulerian hybrid model for the simulation of direct reduction of iron ore in fluidized beds.....	97
High temperature fluidization - influence of inter-particle forces on fluidization behavior	107
Verification of filtered two fluid models for reactive gas-solid flows	115
BIOMECHANICS.....	123
A computational framework involving CFD and data mining tools for analyzing disease in carotid artery	125
Investigating the numerical parameter space for a stenosed patient-specific internal carotid artery model.....	133
Velocity profiles in a 2D model of the left ventricular outflow tract, pathological case study using PIV and CFD modeling.....	139
Oscillatory flow and mass transport in a coronary artery.....	147
Patient specific numerical simulation of flow in the human upper airways for assessing the effect of nasal surgery.....	153
CFD simulations of turbulent flow in the human upper airways	163
OIL & GAS APPLICATIONS	169
Estimation of flow rates and parameters in two-phase stratified and slug flow by an ensemble Kalman filter	171
Direct numerical simulation of proppant transport in a narrow channel for hydraulic fracturing application	179
Multiphase direct numerical simulations (DNS) of oil-water flows through homogeneous porous rocks	185
CFD erosion modelling of blind tees	191
Shape factors inclusion in a one-dimensional, transient two-fluid model for stratified and slug flow simulations in pipes	201
Gas-liquid two-phase flow behavior in terrain-inclined pipelines for wet natural gas transportation	207

NUMERICS, METHODS & CODE DEVELOPMENT	213
Innovative computing for industrially-relevant multiphase flows	215
Development of GPU parallel multiphase flow solver for turbulent slurry flows in cyclone.....	223
Immersed boundary method for the compressible Navier–Stokes equations using high order summation-by-parts difference operators	233
Direct numerical simulation of coupled heat and mass transfer in fluid-solid systems	243
A simulation concept for generic simulation of multi-material flow, using staggered Cartesian grids.....	253
A cartesian cut-cell method, based on formal volume averaging of mass, momentum equations.....	265
SOFT: a framework for semantic interoperability of scientific software	273
POPULATION BALANCE	279
Combined multifluid-population balance method for polydisperse multiphase flows	281
A multifluid-PBE model for a slurry bubble column with bubble size dependent velocity, weight fractions and temperature.....	285
CFD simulation of the droplet size distribution of liquid-liquid emulsions in stirred tank reactors	295
Towards a CFD model for boiling flows: validation of QMOM predictions with TOPFLOW experiments	301
Numerical simulations of turbulent liquid-liquid dispersions with quadrature-based moment methods.....	309
Simulation of dispersion of immiscible fluids in a turbulent couette flow	317
Simulation of gas-liquid flows in separators - a Lagrangian approach.....	325
CFD modelling to predict mass transfer in pulsed sieve plate extraction columns	335
BREAKUP & COALESCENCE	343
Experimental and numerical study on single droplet breakage in turbulent flow	345
Improved collision modelling for liquid metal droplets in a copper slag cleaning process	355
Modelling of bubble dynamics in slag during its hot stage engineering.....	365
Controlled coalescence with local front reconstruction method	373
BUBBLY FLOWS	381
Modelling of fluid dynamics, mass transfer and chemical reaction in bubbly flows	383
Stochastic DSMC model for large scale dense bubbly flows.....	391
On the surfacing mechanism of bubble plumes from subsea gas release.....	399
Bubble generated turbulence in two fluid simulation of bubbly flow	405
HEAT TRANSFER	413
CFD-simulation of boiling in a heated pipe including flow pattern transitions using a multi-field concept	415
The pear-shaped fate of an ice melting front	423
Flow dynamics studies for flexible operation of continuous casters (flow flex cc).....	431
An Euler-Euler model for gas-liquid flows in a coil wound heat exchanger.....	441
NON-NEWTONIAN FLOWS.....	449
Viscoelastic flow simulations in disordered porous media	451
Tire rubber extrudate swell simulation and verification with experiments	459
Front-tracking simulations of bubbles rising in non-Newtonian fluids.....	469
A 2D sediment bed morphodynamics model for turbulent, non-Newtonian, particle-loaded flows.....	479

METALLURGICAL APPLICATIONS.....	491
Experimental modelling of metallurgical processes	493
State of the art: macroscopic modelling approaches for the description of multiphysics phenomena within the electroslag remelting process	499
LES-VOF simulation of turbulent interfacial flow in the continuous casting mold	507
CFD-DEM modelling of blast furnace tapping	515
Multiphase flow modelling of furnace tapholes	521
Numerical predictions of the shape and size of the raceway zone in a blast furnace.....	531
Modelling and measurements in the aluminium industry - Where are the obstacles?	541
Modelling of chemical reactions in metallurgical processes.....	549
Using CFD analysis to optimise top submerged lance furnace geometries	555
Numerical analysis of the temperature distribution in a martensic stainless steel strip during hardening.....	565
Validation of a rapid slag viscosity measurement by CFD.....	575
Solidification modeling with user defined function in ANSYS Fluent.....	583
Cleaning of polycyclic aromatic hydrocarbons (PAH) obtained from ferroalloys plant.....	587
Granular flow described by fictitious fluids: a suitable methodology for process simulations	593
A multiscale numerical approach of the dripping slag in the coke bed zone of a pilot scale Si-Mn furnace.....	599
INDUSTRIAL APPLICATIONS	605
Use of CFD as a design tool for a phosphoric acid plant cooling pond	607
Numerical evaluation of co-firing solid recovered fuel with petroleum coke in a cement rotary kiln: Influence of fuel moisture	613
Experimental and CFD investigation of fractal distributor on a novel plate and frame ion-exchanger	621
COMBUSTION	631
CFD modeling of a commercial-size circle-draft biomass gasifier.....	633
Numerical study of coal particle gasification up to Reynolds numbers of 1000.....	641
Modelling combustion of pulverized coal and alternative carbon materials in the blast furnace raceway	647
Combustion chamber scaling for energy recovery from furnace process gas: waste to value	657
PACKED BED.....	665
Comparison of particle-resolved direct numerical simulation and 1D modelling of catalytic reactions in a packed bed	667
Numerical investigation of particle types influence on packed bed adsorber behaviour	675
CFD based study of dense medium drum separation processes	683
A multi-domain 1D particle-reactor model for packed bed reactor applications.....	689
SPECIES TRANSPORT & INTERFACES	699
Modelling and numerical simulation of surface active species transport - reaction in welding processes	701
Multiscale approach to fully resolved boundary layers using adaptive grids.....	709
Implementation, demonstration and validation of a user-defined wall function for direct precipitation fouling in Ansys Fluent.....	717

FREE SURFACE FLOW & WAVES	727
Unresolved CFD-DEM in environmental engineering: submarine slope stability and other applications.....	729
Influence of the upstream cylinder and wave breaking point on the breaking wave forces on the downstream cylinder	735
Recent developments for the computation of the necessary submergence of pump intakes with free surfaces	743
Parallel multiphase flow software for solving the Navier-Stokes equations	752
PARTICLE METHODS	759
A numerical approach to model aggregate restructuring in shear flow using DEM in Lattice-Boltzmann simulations	761
Adaptive coarse-graining for large-scale DEM simulations.....	773
Novel efficient hybrid-DEM collision integration scheme.....	779
Implementing the kinetic theory of granular flows into the Lagrangian dense discrete phase model.....	785
Importance of the different fluid forces on particle dispersion in fluid phase resonance mixers	791
Large scale modelling of bubble formation and growth in a supersaturated liquid.....	798
FUNDAMENTAL FLUID DYNAMICS	807
Flow past a yawed cylinder of finite length using a fictitious domain method	809
A numerical evaluation of the effect of the electro-magnetic force on bubble flow in aluminium smelting process.....	819
A DNS study of droplet spreading and penetration on a porous medium.....	825
From linear to nonlinear: Transient growth in confined magnetohydrodynamic flows.....	831

RECENT DEVELOPMENTS FOR THE COMPUTATION OF THE NECESSARY SUBMERGENCE OF PUMP INTAKES WITH FREE SURFACES

Frank BLOEMELING*, Ralf LAWALL

TUEV NORD EnSys GmbH & Co. KG, 22525 Hamburg, GERMANY

* E-mail: fbloemeling@tuev-nord.de

ABSTRACT

Swirling flow and gas entrainment induced by vortex formation at pump intakes are possible causes for pump failures and damages. Thus, the avoidance of hollow surface vortices is a safety-related issue for all plants which require a reliable pump operation.

The most efficient measure to avoid these problems is a sufficient submergence of the intake. An acceptable submergence can be determined by means of costly experiments, complex CFD calculations or special correlations. When using correlations their applicability for the specific case has to be taken into account carefully, because a universally applicable correlation is not available yet. Hence, there is a present need for improved correlations or numerical methods which are capable to compute the necessary submergence.

Within the research alliance SAVE experiments and numerical simulations were performed to investigate the occurrence of surface vortices at industrial scales. Amongst others, the lengths of the gas cores of the surface vortices were measured with varying boundary conditions and the velocity fields were determined by means of PIV (Particle Image Velocimetry) measurements. These experiments were accompanied by CFD simulations, the results were compared with the experimental data. A methodology was developed based on single phase CFD simulations with ANSYS CFX in combination with the Burgers-Rott vortex model which can be used to compute the gas core length with very good accuracy. Additionally, two phase CFD simulations were performed which use a free surface model based on recent developments.

In order to develop an improved correlation for the computation of the necessary submergence, which considers in particular the circulation in the approaching flow, several parameter studies were performed. As a result of these studies two new theoretical approaches for the limiting cases of very small and very large circulation were developed which yield new correlations for the computation of the necessary submergence of pump intakes.

Keywords: pump intake design, submergence, free surface flow, surface vortices.

NOMENCLATURE

Greek Symbols

α	Volume fraction, [m ³ /m ³].
γ	Interfacial area density, [1/m].
Γ	Circulation, [m ² /s].
ρ	Mass density, [kg/m ³].
μ_{eff}	Effective dynamic viscosity, [Pa s].
ν	Kinematic viscosity, [m ² /s].
Θ	Interfacial mass transfer, [kg/(m ³ s)].
Ψ	Interfacial momentum transfer, [N/m ³].

Latin Symbols

a	Suction parameter, [1/s].
C_D	Drag coefficient, [-].
d	Suction pipe diameter, [m].
d_V	Vessel diameter, [Pa].
F_D	Drag force, [N/m ³].
g, \mathbf{g}	Gravity acceleration, [m/s ²].
\mathbf{I}	Identity matrix, [-].
h	Submergence, [m].
l	Gas core length, [m].
M	Mass flow rate, [kg/s].
\mathbf{n}	Surface normal vector, [-].
p	Pressure, [Pa].
Q	Volume flow rate, [m ³ /s].
r	Radial coordinate, [m].
r_{max}	Characteristic radius, [m].
\mathbf{S}	Mean strain-rate tensor, [1/s].
t	Time, [s].
\mathbf{u}	Velocity, [m/s].
u	Velocity in the suction pipe, [m/s].
W	Kinetic energy per unit time, [J/s].
z	Axial coordinate, [m].

Dimensionless numbers

A	Dimensionless suction parameter, [-].
Fr	Froude number, [-].
H	Dimensionless submergence, [-].
L	Dimensionless gas core length, [-].
N	Circulation number, [-].

Re Reynolds number, [-].

Sub/superscripts

g, l Gaseous and liquid phase, respectively.

r Radial component.

θ Azimuthal component.

$crit$ Critical.

ref Reference.

INTRODUCTION

In many industrial applications a reliable operation of pumps is required. The applications range from the simple emptying of fluid tanks or tank ships over dewatering or wastewater applications to cooling in the nuclear industry. Depending on their intended use disturbances of the pumps may lead to consequences like production downtimes or even safety-relevant problems, if for instance cooling, fire-extinguishing or dewatering systems are affected.

Since gas entrainment and swirl caused by surface vortices at free surfaces are two main sources of possible pump problems, the occurrence of surface vortices should be prevented. The consequences of swirl and gas entrainment include for instance a decreased flow rate up to a complete blockage of the pump, vibrations, noise and mechanical damage. The most effective measure to avoid surface vortices is a sufficient submergence of the pump intake.

But the necessary submergence depends on several site specific parameters like the intake geometry, the flow rate or the circulation of the inflow. Therefore, a lot of work has been done and is still going on to provide methods to determine the necessary submergence of pump intakes. This includes the design of model experiments and the development of numerical methods as well as easy-to-use correlations.

Although several correlations are available, they are all linked with certain ranges of applicability or boundary conditions, respectively. For instance the American National Standard for pump intake design represented by the Hydraulic Institute recommends the so-called ANSI correlation (Hydraulic Institute, 2012). According to this standard this correlation is only applicable for cases with moderate circulation. A universally applicable and reliable correlation does not exist.

Therefore, the research alliance SAVE investigated the conditions for the occurrence and the shape of surface vortices. Amongst others, the aim was to improve existing design recommendations with particular consideration of the influence of circulation on the surface vortices.

For this purpose an industrial scale experimental facility was built at the Hamburg University of Technology (TUHH) (Szeliga, 2016). The experiments at this facility were used to develop and to validate numerical methods which are able to compute the onset and the shape of surface vortices. Furthermore, the results of the experiments and simulations were used to develop new correlations which can be applied for the determination of the necessary pump submergence.

In the following the experimental setup at the TUHH is presented first. The corresponding single and multi-phase CFD models are explained next. In the subse-

quent section a short overview of selected analytical vortex models is given. These vortex models are used in the following sections which start with the validation of the CFD models. In the next section a theoretical model is proposed which yields new correlations for the determination of the necessary submergence in the presence of strong circulation. Moreover, the new model is validated with available experimental data. Finally also a second model is proposed for the opposite case of very small circulation. This model is confirmed by different parameter studies. The paper closes with a summary and some conclusions.

EXPERIMENTAL SETUP

Many experiments dealing with surface vortices were performed at small scale test facilities. In order to exclude scaling effects from the outset, a test facility was built at the TUHH that on one hand has typical industrial dimensions and on the other hand is flexible enough to allow the examination of all relevant parameters which affect the surface vortices. The test facility consists mainly of a large cylindrical vessel with 4 m diameter and 4 m height (see figure 1).

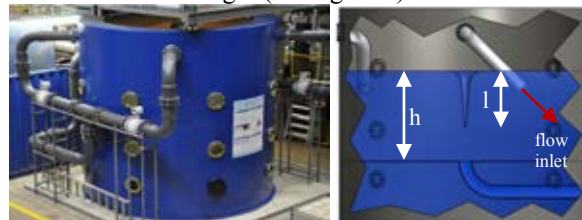


Figure 1: Test facility at the TUHH (left: exterior view; right: sketch of the interior) (Szeliga, 2016)

The water enters the test vessel via four adjustable DN200 inlet pipes. The water jets from these pipes generate an angular momentum, which causes a circulation that depends on the pipes' inclination. The pump suction intake is located at the centre of an intermediate floor. Its shape can be altered in order to examine the influence of the intake geometry. The basic configuration is a flush mounted suction pipe with 0.2 m inner diameter. Optical measurements are possible through small windows in the vessel. Due to the symmetrical setup different types of stable, hollow vortices can be generated in the centre of the vessel. The types range from swirl without any surface deformation to fully developed gas cores which reach into the suction line. Gas cores whose lengths equal exactly the submergence are of particular importance. They characterise the so-called critical submergence. Submergences lower than the critical one usually lead to continuous gas entrainment into the pump.

Among others, the gas core lengths as well as the tangential fluid velocities were measured during the experiments under varying boundary conditions.

CFD MODELS

To numerically analyse the experiments different CFD models were set up with ANSYS CFX. First a single-phase model was built that simulates only the liquid phase. Compared to two-phase simulations this approach is much less computationally expensive. But a direct computation of a surface deformation is not pos-

sible by applying this kind of simulations. Therefore, additionally a two-phase model was developed that considers also the gaseous phase and is capable to track the water surface.

Single-phase model

The single-phase model consists only of the liquid phase (water at 20° C). The geometry and the boundary conditions are shown in figure 2. Because of symmetry only a model of a quarter of the test vessel geometry is required. At the vertical cut planes a rotational periodicity is used. A mass flow rate and a pressure boundary condition define the inlet and the outlet, respectively. The water surface at 1.467 m is replaced by a non-deformable free slip wall at which the water can move freely in azimuthal and radial direction.

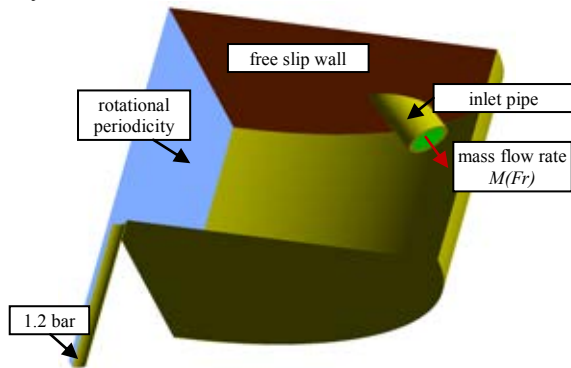


Figure 2: Single-phase CFD model

The underlying equations are the incompressible Reynolds averaged Navier-Stokes equations (RANS) (Wilcox, 1993). Thus, the influence of turbulence is modelled by the Reynolds stress tensor in the momentum equations. To close the system of equations the Shear Stress Transport model (SST) is used with automatic wall functions. The SST model is a two equation turbulence model based on the turbulent kinetic energy and the turbulent dissipation frequency (Menter, 1994). It is crucial to turn on the built-in curvature correction (Spalart and Shur, 1997), because otherwise the SST model is not an appropriate choice for strongly swirling flow. The curvature correction considers the swirling flow and enhances or damps the turbulence production appropriately.

ANSYS CFX applies a co-located, vertex-centered Finite Volume Method (ANSYS, 2016). In the present case a high resolution scheme is used to discretise the advection terms of the conservation equations and the transient parts are discretised by an implicit second order Euler method.

In figure 3 the grid is shown that is mainly structured and consists of hexahedral cells. Only the vicinity of the inclined inlet pipe is meshed with tetrahedral cells in order to achieve a better grid quality. The grid is locally refined at walls and the vessel centre. The maximum edge length is 40 mm. In the centre the grid resolution is much finer. The horizontal edge length in this region is between 3 and 4 mm. Altogether the grid contains ca. 0.5 million cells.

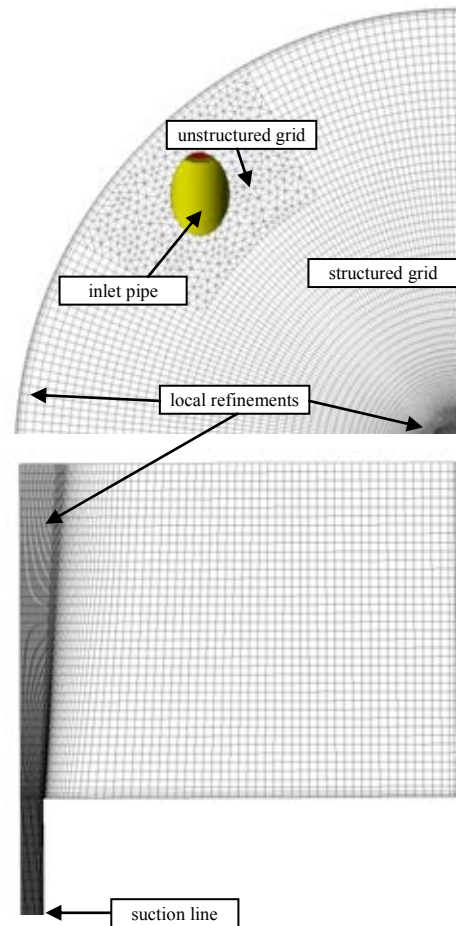


Figure 3: Computational grid (top and side view)

Two-phase model

In the two-phase case both the liquid phase and the gaseous phase above the free surface are modelled (water and air). Therefore, it is necessary to extend the model by an air domain above the water surface (see figure 4). The air is treated as an ideal gas. In contrast to the single-phase model the top is now modelled by a no-slip wall. The other boundary conditions remain unchanged. The air domain is obtained by extruding the grid shown in figure 3. Thus, the principle grid structure and the grid quality do not change.

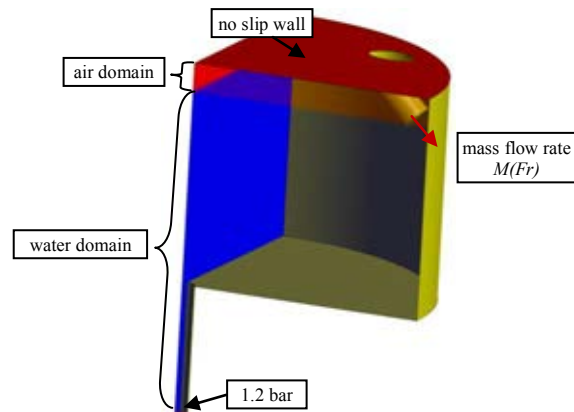


Figure 4: Two-phase CFD model

In the two-phase model each phase has its own continuity and momentum equation which now contain the volume fractions α_g and α_l of the gaseous and liquid phase, respectively. Furthermore, the terms Θ_k and Ψ_k

for interfacial mass and momentum transfer are included.

Continuity equation:

$$\frac{\partial(\alpha_k \rho_k)}{\partial t} + \nabla \cdot (\alpha_k \rho_k \mathbf{u}) = \Theta_k \quad (1)$$

Momentum equation:

$$\frac{\partial(\alpha_k \rho_k \mathbf{u}_k)}{\partial t} + \nabla \cdot (\alpha_k \rho_k \mathbf{u}_k \otimes \mathbf{u}_k) = -\alpha_k \nabla p + \nabla \cdot (\alpha_k \mu_{eff,k} \mathbf{S}_k) + \alpha_k \rho_k \mathbf{g} + \Psi_k \quad (2)$$

with $k \in \{g, l\}$ and

$$\mathbf{S}_k = \nabla \mathbf{u}_k + \nabla \mathbf{u}_k^T - \frac{2}{3} (\nabla \cdot \mathbf{u}_k) \mathbf{I}$$

is the main strain-rate tensor. Since no mass transfer occurs between the two phases, the transfer term Θ_k vanishes.

Although there were several successful attempts in the past to use the Volume-of-Fluid Method in order to simulate hollow surface vortices (Ito, 2010a, or Merzari, 2008), the above Two-Fluid Model was chosen in this case. The main reason is that recent developments show that this model can be applied successfully in order to cover different flow regimes simultaneously (Haensch, 2012). Thus, it is a promising candidate for future simulations that aim to quantify the gas entrainment, since this involves free surface and dispersed flow regimes. The use of the Volume-of-Fluid Method for this purpose is probably too costly, since also small bubbles have to be resolved.

For the computation of the remaining momentum transfer term the concept of the Algebraic Interfacial Area Density Model (AIAD) (Hoehne, 2011) was adopted. In the case of free surface flows ANSYS CFX computes the interfacial area density from the volume fraction gradient

$$\gamma = \|\nabla \alpha\| \quad (3)$$

and the momentum transfer is

$$\Psi_f = C_D (\alpha_g \rho_g + \alpha_l \rho_l) \gamma \|\mathbf{u}_g - \mathbf{u}_l\| (\mathbf{u}_g - \mathbf{u}_l). \quad (4)$$

Equation (4) describes an interfacial drag force that is dependent on the drag coefficient C_D . This drag coefficient is computed in the AIAD model, as if the water surface acted like a wall. Then the phase specific drag force $\mathbf{F}_{D,k}$ can be computed via

$$\mathbf{F}_{D,k} = \gamma \mu_k (\mathbf{I} - \mathbf{n}_k \otimes \mathbf{n}_k) \mathbf{S}_k \cdot \mathbf{n}_k \quad (5)$$

with the surface normal vector

$$\mathbf{n}_k = -\frac{\nabla \alpha_k}{\gamma}. \quad (6)$$

So finally the drag coefficient can be calculated from

$$C_D (\alpha_g \rho_g + \alpha_l \rho_l) \gamma \|\mathbf{u}_g - \mathbf{u}_l\|^2 = \alpha_g \|\mathbf{F}_{D,g}\| + \alpha_l \|\mathbf{F}_{D,l}\|. \quad (7)$$

The other settings are very similar to the single-phase case. For instance the SST turbulence model with curvature correction is used again. However, the time step has to be chosen much smaller than in the single-phase simulations in order to keep the Courant number smaller than one. This makes the two-phase simulations very time consuming. However, some time can be saved, when a single-phase simulation is used as initial conditions.

ANALYTICAL VORTEX MODELS

As already mentioned it is not possible to determine any surface deformation with the single-phase model. But by means of an analytical vortex model this situation can be remedied.

The probably simplest vortex model is the Rankine model (Wu et. al, 2006) that divides the vortex into two regions, an outer free vortex region and a core region. The core region behaves like a rotating solid. Therefore, the tangential velocity of the vortex can be expressed by

$$u_\theta = \frac{\Gamma}{2\pi r} \begin{cases} 1, & \text{for } r \geq r_{max} \\ \left(\frac{r}{r_{max}}\right)^2, & \text{for } r < r_{max}. \end{cases} \quad (8)$$

The model depends on the parameter r_{max} that characterises the location, where the velocity attains its maximum. Furthermore, the model depends on the circulation Γ .

A more evolved model is the model of Burgers and Rott (Rott, 1958). It describes a rotationally symmetrical stagnation-point flow. Inserting this assumption into the Navier-Stokes equations leads to the following tangential velocity.

$$u_\theta = \frac{\Gamma}{2\pi r} \left[1 - \exp\left(-a \frac{r^2}{4\nu}\right) \right]. \quad (9)$$

Again, two parameters have to be provided by the user of equation (9). Beside the circulation Γ the so-called suction parameter (or downward velocity gradient) a has to be specified. The suction parameter is related to r_{max} via the equation

$$\frac{r_{max}}{1.1209} = 2 \sqrt{\frac{\nu}{a}}. \quad (10)$$

Note that the shape of the water surface is characterised by a constant pressure condition. By applying this condition one obtains the ordinary differential equation

$$\frac{dz}{dr} = -\frac{u_\theta^2}{g r} \quad (11)$$

that describes the deflection of the water surface. Substituting equation (9) in equation (11) and integration yields the formula

$$l = \frac{a \ln(2)}{\nu g} \left(\frac{\Gamma}{4\pi} \right)^2 \quad (12)$$

for the gas core length of surface vortices (Ito, 2010). The difficulty with the application of the analytical vortex model of Burgers and Rott is the determination of the parameters circulation Γ and suction parameter a for arbitrary or even for simple intake geometries. For this task CFD is an excellent tool. By determining the circulation and the suction parameter from the CFD results and by applying equation (9) or (12), respectively, it is possible to compute the shape and the length of gas cores of hollow vortices. This is even possible, if only single-phase CFD simulations are performed, which require much less effort compared to two-phase models.

There exist several other analytical vortex models of comparable complexity. But there are also attempts to obtain a more general description of vortex flow. One is given by Granger who developed a sequence of systems of partial differential equations resulting from a power series expansion based on the radial Reynolds number (Granger, 1966). The 0th order model of Granger, i.e. the

first term of the power series, consists of two partial differential equations for the dimensionless stream function and the dimensionless circulation. The solution of these partial differential equations requires the knowledge of the centre line distribution of vorticity and axial velocity or alternatively the application of numerical methods. In the present case the 0th order Granger model was used in parameter studies and the equations were solved with a second order finite difference method.

VALIDATION OF THE CFD MODELS

The single-phase CFD model in combination with the Burgers-Rott vortex model as well as the two-phase CFD model were validated by the comparison of gas core lengths and tangential velocities with corresponding experimental measurements.

Figure 5 shows the tangential velocities determined with the single-phase CFD model for Froude number

$$Fr = \frac{u}{\sqrt{g d}} = 1.2. \tag{13}$$

This Froude number corresponds to a total mass flow of 53 kg/s. At this mass flow the submergence became critical in the experiments. The computed tangential velocities are evaluated along three lines at different elevations. There are only slight differences in the core region of the vortex between these positions. Additionally, the tangential velocities according to the Burgers-Rott model with adjusted parameters are included in the figure. The Burgers-Rott model agrees well with the CFD results.

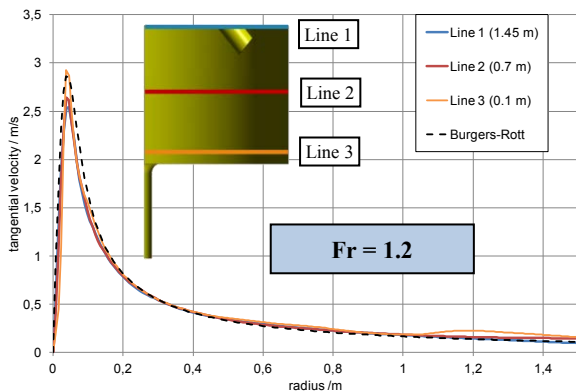


Figure 5: Tangential velocities according to CFX and the Burgers-Rott vortex model; Fr = 1.2

Once the parameters of the Burgers-Rott model are determined equations (11) and (12) can be used to compute the gas core shape. Figure 6 shows the gas core shapes, which are determined by the vortex model of Burgers and Rott, for two different mass flows and the maximal deflection of the water surface observed in the corresponding experiments. In both cases the length of the gas cores matches the experimental data with very good accuracy. Even the critical conditions at Fr = 1.2, for which the gas cores lengths equal exactly the submergence, are well predicted.

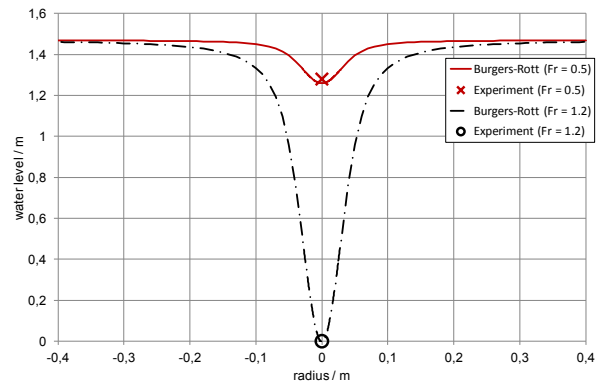


Figure 6: Gas core shapes for different mass flows

For the case with lower Froude number (Fr = 0.5) measurements of the tangential velocities are available (Szeliga, 2016). They were obtained by Particle Image Velocimetry (PIV). A comparison of the measurements and the CFD simulation results is presented in figure 7. Obviously also the measured and computed tangential velocities coincide well.

So far it was demonstrated that the combination of single-phase CFD simulations with the Burgers-Rott model is an accurate approach for the determination of the gas core length. Therefore, the attention is now turned on the two-phase model that allows the computation of the water surface directly without applying an analytical vortex model.

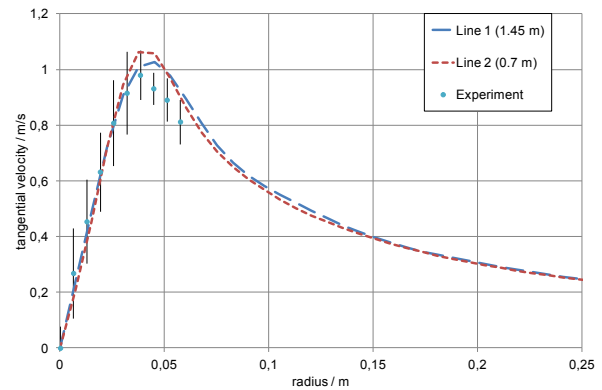


Figure 7: Comparison between measured and computed tangential velocities, Fr = 0.5

For the two-phase simulations a Froude number Fr = 1 was used, corresponding to 45 kg/s mass flow. Thus, critical conditions are not reached yet, but the experimentally observed gas core length of the surface vortex is about 70 % of the submergence. To simplify the simulations they were started with the single-phase results as initial conditions. After a simulation time of approximately 1 s an elongated gas core was formed during the simulations which corresponds very well with the experimental observations and the Burgers-Rott model (see figure 8). By continuing the simulation it turned out that the gas core became thinner and tore off at some point. As a consequence the surface vortex vanishes and has to develop again. However, the two-phase model has proved its suitability and ability to reproduce the shape of the surface vortex.

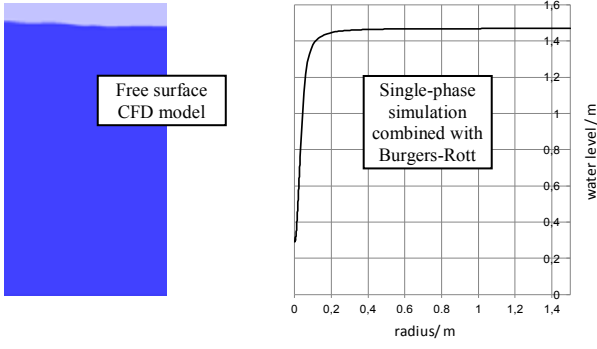


Figure 8: Comparison between CFD simulation (left) and Burgers-Rott model (right)

COMPUTATION OF THE GAS CORE LENGTH AND THE NECESSARY SUBMERGENCE IN THE PRESENCE OF LARGE CIRCULATION

According to equation (12) the computation of the gas core length of a surface vortex requires the knowledge of the circulation Γ and the suction parameter a . The circulation is a parameter that depends strongly on the specific geometry. For the TUHH experiment the CFD simulations reveal an affine linear relationship between the angular momentum induced by the inlet pipes and the circulation in the vessel. This relation can be expressed for a given submergence and inclination of the inlet pipes by a simple equation. For instance the formula

$$\frac{\Gamma}{m^2/s} = (0.258 + 0.542 Fr^2) \quad (14)$$

can be derived for a submergence of 1.467 m and inlet pipes that are inclined at an angle of 45° .

While the circulation is highly system-dependent the suction parameter can be obtained by a theoretical approach that is described in the following.

A rotating fluid without any suction behaves like a rotating solid, because in this case the kinetic energy attains a minimum for a given circulation. This can be easily demonstrated with the Rankine model in equation (8). Enlarging r_{max} reduces the tangential velocities. Therefore, the kinetic energy in the cylindrical vessel reaches a minimum, if r_{max} attains a maximum, e.g. $r_{max} = d_v / 2$. In this case the entire fluid can be interpreted as solid body. But pumping changes the character of the flow. The typical tangential velocity profile (cmp. figure 5) consisting of a free vortex and a solid body rotation appears. This happens because a certain portion of kinetic energy is detracted from the vessel through the suction line. However, to sustain the rotation with the same circulation it is necessary that the rotating fluid also contains this additional portion of kinetic energy. This can be controlled by the parameter r_{max} .

The kinetic energy per unit time which is detracted through the suction line can be expressed by

$$\Delta W = \frac{\rho}{2} \frac{Q^3}{(\pi/4 d^2)^2}. \quad (15)$$

Because in strongly rotating flow the tangential velocity dominates the axial and radial velocities, the radial and axial components can be neglected in the cylindrical vessel. Therefore, the kinetic energy that passes a certain radius per unit time becomes

$$W = \frac{\rho}{2} Q u_0^2. \quad (16)$$

As explained this expression becomes minimal, if the characteristic radius is chosen as half of the cylinder diameter which yields the reference kinetic energy per unit time

$$W_{ref} = \frac{\rho}{2} Q \left(\frac{\Gamma}{\pi d_v} \right)^2 \left(\frac{2r}{d_v} \right)^2. \quad (17)$$

By subtracting equation (17) from equation (16) and evaluation at $r = r_{max}$ one obtains

$$(W - W_{ref})_{r=r_{max}} = \frac{\rho}{2} Q \left(\frac{\Gamma}{\pi d_v} \right)^2 \left(\left(\frac{d_v}{2r_{max}} \right)^2 - \left(\frac{2r_{max}}{d_v} \right)^2 \right) \quad (18)$$

for the additional energy flux resulting from a certain choice of the parameter r_{max} . This additional flux must equal the expression in equation (15) to compensate the loss of energy through the suction line. This condition finally leads to the equation

$$\left(4 \frac{Q}{d^2} \frac{d_v}{\Gamma} \right)^2 = \frac{1 - \xi^4}{\xi^2}, \quad \text{with } \xi := \frac{2r_{max}}{d_v} \quad (19)$$

which is a quadratic equation in ξ^2 with the solution

$$\xi = \sqrt{\sqrt{1 + \frac{\varepsilon^2}{4}} - \frac{\varepsilon}{2}}, \quad \text{with } \varepsilon := \left(0.25 \frac{d}{d_v} N \right)^{-2}. \quad (20)$$

In the above equation (20) the circulation Γ has been replaced by the dimensionless circulation number

$$N = \frac{\Gamma d}{Q}. \quad (21)$$

The Rankine model is a model with simplifications and it doesn't yield the correct kinetic energy distribution. For this reason a correction factor $\kappa = 0.41$ is introduced, when the parameter r_{max} is determined from the definition of ξ , i.e.

$$r_{max} = \kappa \frac{d_v}{2} \xi. \quad (22)$$

The correction factor is derived from the experimental data. Now the suction parameter a can be computed with equation (10).

Usually it is preferable to use dimensionless quantities. The dimensionless suction parameter A can be defined by

$$A = \frac{a d^3}{Q}. \quad (23)$$

Substituting equation (10) and rewriting equation (22) by using equation (23) leads to the dimensionless equation

$$A = \frac{150}{Re} \frac{1}{\xi^2} \left(\frac{d}{d_v} \right)^2, \quad (24)$$

where Re denotes the Reynolds number

$$Re = \frac{u d}{\nu}. \quad (25)$$

Note that equation (20) is already written in dimensionless form.

The dimensionless version of equation (12) is given by

$$L = \frac{\pi \ln(2)}{4^5} A Re Fr^2 N^2. \quad (26)$$

Equation (26) contains two more dimensionless quantities, i.e. the dimensionless gas core length

$$L = \frac{l}{d} \quad (27)$$

and the Froude number.

The equations (26), (24) and (20) form a new mathematical model for the computation of the gas core length which uses the Reynolds, Froude and circulation number as input parameters. This new model is applicable for surface vortices with strong circulation. Note that the circulation number depends on the circulation which therefore has to be given for instance by a relation like equation (14).

In the following the model is validated with the experimental data gained from the TUHH experiments and with data from the independent experiment of Moriya (Ito, 2010).

Figure 9 shows a comparison of the theoretical gas core lengths obtained from equation (26) with experimentally observed gas core lengths from the TUHH. The accuracy of the theory is very good in particular for larger gas cores.

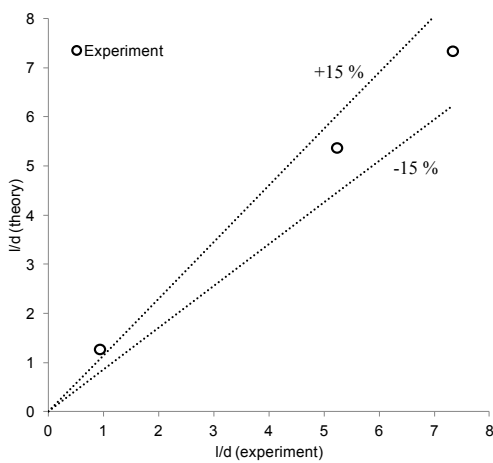


Figure 9: Theoretical vs. experimental gas core lengths; TUHH experiments for Froude numbers $Fr = 0.5, 1, 1.2$

In order to compare the theory also with independent measurements the experiment of Moriya was additionally considered. The setup of this experiment is similar to the TUHH experiments. The test facility consists also of a cylindrical vessel with a vertical pump suction intake (see figure 10). The main differences are the dimensions and the flow inlet. In Moriya’s experiment the water enters the test vessel tangentially through an inlet slit that causes the circulation in the vessel. The circulation is known (equation (41) in the paper of Ito, 2010) and it depends solely on the volume flow rate for fixed submergence.

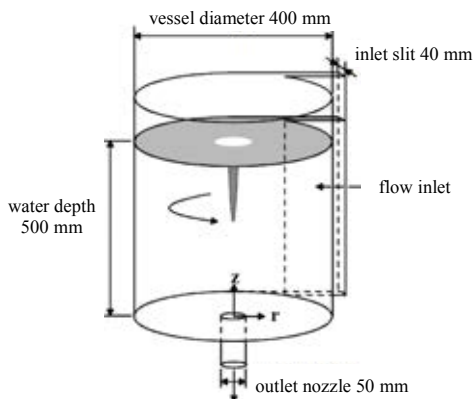


Figure 10: Moriya’s experiment (Ito, 2010)

So, the circulation number N is already given via equation (21). The second parameter, the suction parameter A , can be computed with the above theory (equation (24)). Afterwards the gas core length follows from equation (26). The results are plotted in figure 11.

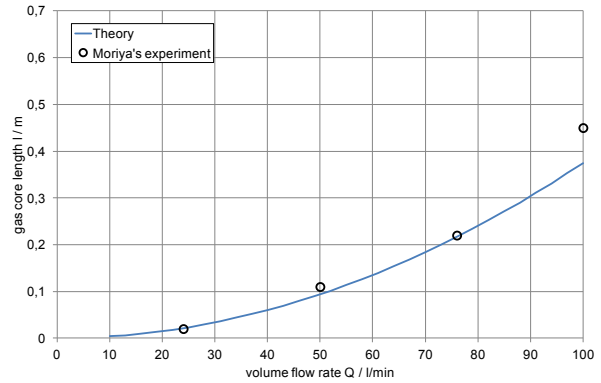


Figure 11: Validation against Moriya’s experiment

Again the theory matches the experimental data with very good accuracy. Only at a high flow rate of 100 l/min the theory deviates slightly from the corresponding measurement.

Since the developed theory allows the determination of the gas core length, only a small modification of equation (26) yields a new correlation for the computation of the critical submergence. By definition the critical submergence is reached, if the gas core length equals the submergence, i.e. $l = h$. Therefore, the dimensionless critical submergence $H_{crit} = h_{crit}/d$ results from equation (26) by simply setting

$$H_{crit} = \frac{\pi \ln(2)}{4^5} A Re Fr^2 N^2. \quad (28)$$

The suction parameter A and the circulation number N are in general functions of the submergence, i.e.

$$A = A(H_{crit}), N = N(H_{crit}). \quad (29)$$

This is a nonlinear implicit equation that has to be solved for H_{crit} .

EXTENSION OF THE THEORY TO SMALL AND MODERATE CIRCULATION

The theoretical approach that leads to the suction parameter in equation (24) is valid for strongly circulating flow. Therefore, it is applicable to the TUHH experiments and Moriya’s experiment. To examine if it is also suitable for moderate circulation further parameter studies were performed.

So firstly, cases without any circulation were investigated. For this purpose the 0th order Granger model was solved with a second order finite difference method. This procedure was chosen, because it allows the variation of the suction line diameter and the submergence without the necessity of complex remeshing steps.

The variations of the submergence and the suction line diameter in the Granger model reveal a relationship between the dimensionless suction parameter A and the dimensionless submergence H that fits very well to the equation

$$A = 1.1 H^{-2.88}. \quad (30)$$

Both the results from the Granger model and the graph of the derived correlation are shown in figure 12.

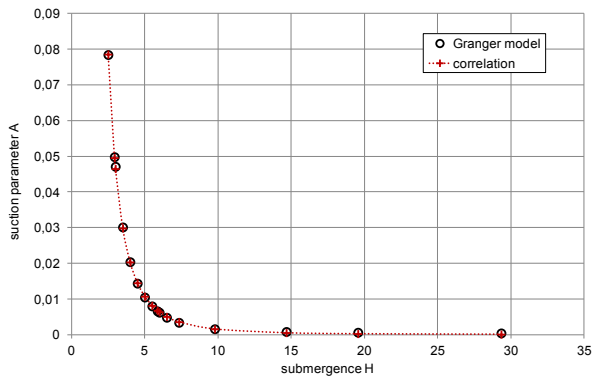


Figure 12: Suction parameter in dependency of the submergence (cases without circulation)

Since the applied finite difference solver of the Granger model considers no circulation, more parameter studies were performed with another generic ANSYS CFX model. This generic model consists of a simple cylindrical domain, but it is possible to generate a specified moderate circulation by imposing an inflow angle at the circumference. All parameter studies as a whole yield a correlation for cases with small circulation which is given by the following equation

$$A = 1.1 H^{-2.88} \left(1 - \frac{2 \arctan(NH)}{\pi} \right). \quad (31)$$

Equation (24) and equation (31) represent two different correlations developed for the limiting cases of large and small circulation. The corresponding graphs for a pump intake diameter of 0.2 m, 45 kg/s mass flow and a submergence of 1.467 m as well as varying circulation numbers are plotted in figure 13.

Obviously the theory for small circulation fits well to the simulations with the Granger model and the generic CFX model, while the theory for large circulation fits well to the simulation of the TUHH experiment with an inlet pipe inclination of 45°. Hence, both theories are confirmed by CFD simulations and in particular the theory for large circulation is also validated with experimental results. Moreover, the experimental data of Jain (1978) indicates that the desired suction parameter for moderate circulation lies indeed between both theories. Therefore, an appropriate interpolation between both theories is required to capture the correct suction parameter in cases with moderate circulation. This will be the topic of future investigations.

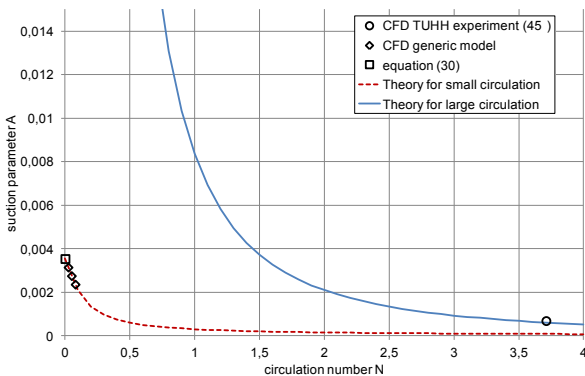


Figure 13: Dimensionless suction parameter over circulation number according to the theories of large and small circulation

SUMMARY AND CONCLUSIONS

The avoidance of gas entrainment and a homogenous flow without swirl are basic requirements for an undisturbed pump operation. As a consequence surface vortices, which might occur at free surfaces, have to be prevented. The most effective measure in this regard is a sufficient submergence of the intake. But the determination of the critical submergence requires either elaborate model experiments or estimations by means of some correlation. Due to the lack of an universally applicable and reliable correlation, there is an ongoing need for improved correlations.

Therefore, an industrial scale test facility has been built at the TUHH in order to examine the conditions for the occurrence and the shape of surface vortices. In particular the length of gas cores of those hollow vortices was analysed with varying boundary conditions. The so gained experimental data was used to develop appropriate strategies for the computation of the gas core lengths, the vortex shapes and therefore also the critical submergence. Numerical methods were applied based on single- and multi-phase CFD models. The multiphase CFD approach has shown its ability to calculate the shape of the gas cores directly, but the computational effort of the multiphase simulations is very high. In fact, it turned out that it is possible to accurately compute the shape of the surface vortices with single-phase CFD simulations in combination with the Burgers-Rott vortex model that is a much more efficient approach. Both methods were applied to simulate the TUHH experiments and they were validated with the corresponding measurements.

Furthermore, two new theories have been developed which yield new correlations for the computation of the gas core length of surface vortices and the critical submergence, respectively. The first theory results from an energy balance and is applicable for flows with strong circulation. In addition it was validated with the TUHH experiments and the independent experiment of Moriya. The second approach is based on parameter studies with CFD and yields a correlation for flows with very low circulation. These theories represent the two limiting cases for swirling flows. Cases with moderate circulation like Jain’s experiment lie in between and require an adequate interpolation between both theories.

ACKNOWLEDGMENTS

This work is sponsored by the German Federal Ministry of Education and Research (BMBF) under the contract number 02NUK023C. The responsibility for the content of this publication lies with the author.

REFERENCES

- ANSYS Germany GmbH, (2016), ANSYS CFX 17, <http://www.ansys.com/products/fluids/ansys-cfx>
- GRANGER, R., (1966), “Steady three-dimensional vortex flow”, *J. Fluid Mech.*, **25** (3), 557-576
- HAENSCH, S., (2012), “A multi-field two-fluid concept for transition between different scales of interfacial structures”, *International Journal of Multiphase Flow*, **47**, 171-182
- HOEHNE, T., et al., (2011), “Numerical simulations of counter-current two-phase flow experiments in a PWR hot leg

- model using an interfacial area density model”, *International Journal of Heat and Fluid Flow*, **32**, 1047-1056
- HYDRAULIC INSTITUTE, (2012), “Rotodynamic Pumps”, ISBN 978-880952-70-2
- ITO, K. et al., (2010), “Improvement of Gas Entrainment Prediction Method –Introduction of Surface Tension Effect–”, *Journal of Nuclear Science and Technology*, **47 (9)**, 771-778
- ITO, K. et al., (2010a), “CFD-based Evaluation of Interfacial Flows”, *INTECH*, Croatia
- JAIN, A.K. et al., (1978), “Vortex Formation at Vertical Pipe Intakes”, *Journal of the Hydraulics Division*, **HY10**, 1429-1445
- MENTER, F.R., (1994), “Two-Equation Eddy-Viscosity Turbulence Models for Engineering Applications”, *AIAA Journal*, **32 (8)**, 1598-1605, August 1994
- MERZARI, E. et al., (2008), “Numerical Simulation of Free-Surface Vortices”, *Nuclear Technology*, **165**, 313-320
- ROTT, N., (1958), “On the Viscous Core of a Line Vortex”, *Journal of Applied Mathematics and Physics (ZAMP)*, **9**, 543-553
- SPALART, P.R. and SHUR, M., (1997), “On the Sensitization of Turbulence Models to Rotation and Curvature”, *Aerospace Science and Technology*, **4**, 297-302
- SZELIGA, N. et al., (2016), “Determination of the Influence of Tangential Momentum on Air-Core Vortex Formation at Pump Intakes by Means of Particle Image Velocimetry”, *GALA 2016*, 30-1 – 30-9, ISBN: 978-3-9816764-2-6.12
- WILCOX, D.C., (1993), “Turbulence Modelling for CFD”, DCW Industries, Inc., ISBN 0-9636051-0-0
- WU, J.-Z. and MA, H.-Y. and ZHOU, M.-D., (2006), “Vorticity and Vortex Dynamics”, Springer